ISSN 0036-0244, Russian Journal of Physical Chemistry A, 2017, Vol. 91, No. 13, pp. 2651–2656. © Pleiades Publishing, Ltd., 2017.

PHYSICAL CHEMISTRY OF NANOCLUSTERS AND NANOMATERIALS

Effects of Cobalt Doping on the Microstructure and Optical Properties of $ZnAl_2O_4$ Nanoparticles[1]

Xiaojuan Wu[a,b], Zhiqiang Wei[a,b,*], Xiujuan Chen[a], Xuan Wang[b], Hua Yang[a,b], Jinlong Jiang[a], and Lihua Yuan[a]

[a] *State Key Laboratory of Advanced Processing and Recycling Nonferrous Metals, Lanzhou University of Technology, Lanzhou 730050, P.R. China*

[b] *School of Science, Lanzhou University of Technology, Lanzhou 730050, P.R. China*

**e-mail: qianweizuo@163.com*

Received August 31, 2016

Abstract—Co-doped $ZnAl_2O_4$ nanoparticles were prepared by hydrothermal method. The samples were characterized by XRD, HRTEM, EDX, FT-IR, XPS, PL, and UV–Vis, and the effects of cobalt doping on the microstructure and optical property of the samples were studied. The experimental results showed that Co-doped $ZnAl_2O_4$ nanoparticles synthesized by this method are single phase with cubic crystal structure, no other impurity phases were observed. Furthermore, with increasing the Co^{2+} concentration, the average crystallite size of the Co-doped samples became smaller. The absorption bands in FT-IR spectra are broadened in the low frequency region, the PL spectra had the red-shift and the UV–Vis peaks intensity gradually enhanced.

Keywords: $ZnAl_2O_4$, Co-doped, hydrothermal method, microstructure, optical property

DOI: 10.1134/S0036024417130283

INTRODUCTION

Spinel structure materials have attracted many people due to their thermal stability [1], magnetic [2], electronic [3], optical properties [4], and so on. They have an ideal formula AB_2O_4, where (A) represents the divalent metal ions (cations) occupying FCC tetrahedral sites and (B) represents trivalent metal ions (cations) occupying FCC octahedral sites of a cubic crystal structure. Among the most interesting materials of this kind, zinc aluminate ($ZnAl_2O_4$), belonging to *Fd*3*m* space group, is a direct wide band gap semiconductor with an optical band gap value of about 3.8 eV. In recent years, $ZnAl_2O_4$ spinel has been paid much attention due to its usefulness in ceramic, electronic, optical, catalyst, dielectric, and sensing applications [5–9] and so on. This spinel offers many advantageous properties such as high mechanical and thermal resistance, high chemical and thermal stability, low temperature sinterability, hydrophobic behavior, low surface acidity, better diffusion and high quantum yields.

However, transition metal elements doped into the $ZnAl_2O_4$ is of great interest to investigate. when an active dopant is introduced into these spinels, the microstructure and band structure are affected, then their optical and magnetic properties are dramatically changed depending on its distribution in the spinel. In order to clarify this problem, transition metal elements doped $ZnAl_2O_4$ were prepared by various methods, such as, sol–gel method [10, 11], microwave combustion method [12], hydrothermal method [13], the coprecipitation method [14], and so on. Among these methods, the hydrothermal method is easy and provides high purity, good crystallinity and dispersity of the samples; the experimental procedure is also easy to be controlled.

In this paper, $Zn_{1-x}Co_xAl_2O_4$ (x = 0, 0.10, 0.20, and 0.40) were synthesized by hydrothermal method. The crystal structure, morphology and optical of the samples were characterized by XRD, HRTEM, EDX, FT-IR, XPS, PL, and UV–Vis, respectively.

EXPERIMENTAL

Preparation of $Zn_{1-x}Co_xAl_2O_4$ Nanoparticles

$Zn_{1-x}Co_xAl_2O_4$ nanoparticles (x = 0, 0.10, 0.20, and 0.40) were prepared by hydrothermal method from $Zn(NO_3)_2 \cdot 6H_2O$ and $Co(NO_3)_2 \cdot 6H_2O$ with given atomic ratios in distilled water. In a typical synthesis, 4 mmol $Zn(NO_3)_2 \cdot 6H_2O$ and 8 mmol $Al(NO_3)_3 \cdot 9H_2O$ with variable concentrations of 0, 10, 20, and 40% of $Co(NO_3)_2 \cdot 6H_2O$ were diluted with 60 mL distilled water. NaOH (40 mmol) dissolved in 40 mL distilled water was introduced into above solu-

[1] The article is published in the original.

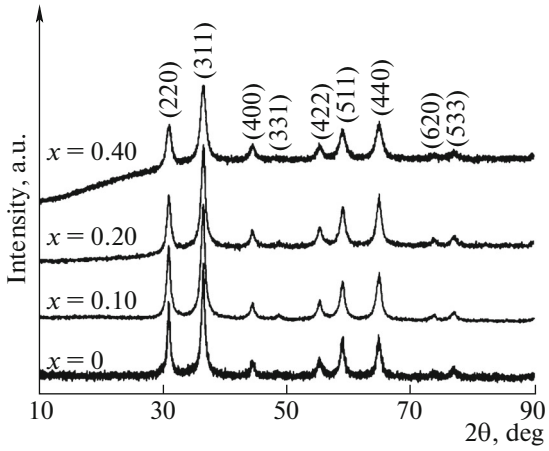

Fig. 1. XRD diffraction patterns of $Zn_{1-x}Co_xAl_2O_4$ (x = 0, 0.10, 0.20, and 0.40) samples.

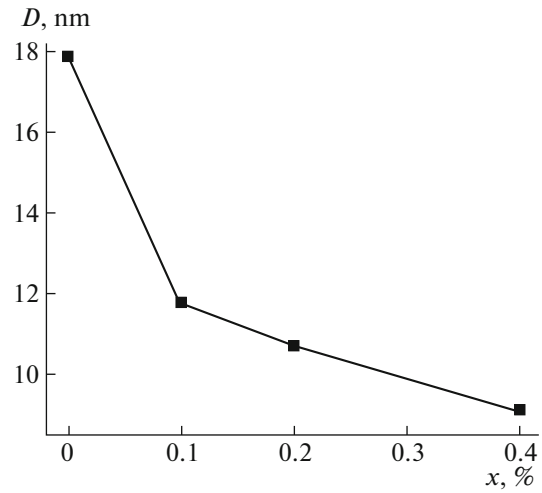

Fig. 2. The grain size D of $Zn_{1-x}Co_xAl_2O_4$ (x = 0, 0.10, 0.20, and 0.40) samples.

tion under magnetic stirring, followed by addition 1 g CTAB. Every step mentioned above was accompanied by constant magnetic stirring. After the solution mixed uniformly, and then transferred to a Teflon-lined stainless autoclave of 100 mL capacity. The hydrothermal process was conducted at 200°C for 24 h. After the reaction, the resulting white precipitates were filtered off, washed with distilled water and absolute ethanol for several times, and then dried under at 60°C for 12 h in air.

Characterization Techniques

X-ray powder diffraction (XRD) patterns of the samples were obtained on Rigaku (Japan) X-ray diffractometer with CuK_α radiation (λ = 1.5418 Å); Transmission electron microscopy (TEM) micrographs were taken using FEI Tecnai G2 F30 instrument; Fourier transform infrared spectroscopy (FT-IR) was carried out on Nexus 670 FT-IR spectrometer; X-ray photoelectron spectrum (XPS) measurements were carried out using a PHI-5702 multifunctional X-ray photoelectron spectroscope (XPS) under AlK_α radiation; Photoluminescence (PL) spectra were obtained on a PerkinElmer spectrophotometer (LS-55) with a He–Cd laser as excitation source; the ultraviolet–visible (UV–Vis) spectra were recorded on a spectrophotometer with an integrating sphere attachment.

RESULTS AND DISCUSSION

The XRD patterns of $Zn_{1-x}Co_xAl_2O_4$ (x = 0, 0.10, 0.20, and 0.40) are shown in Fig. 1. As seen in Fig. 1, all diffraction peaks of $Zn_{1-x}Co_xAl_2O_4$ are consistent with the standard values of the spinel $ZnAl_2O_4$ with cubic structure (JCPDS card no. 05-0669). It is easy to find from the spectrum that no impurities were detected when Co^{2+} content increased from 0 to 40%. These peaks can be indexed as (220), (311), (400), (331), (422), (511), (440), (620), and (533) diffraction lines. With increasing the Co^{2+} concentration, the half-width became gradually widened. The grain size had been calculated using Debye–Scherrer's formula: $D = \frac{K\lambda}{B\cos\theta}$, where D is the grain size; λ is the wavelength of the X-ray source (CuK_α, 1.54056 Å); β is the corrected full width at maximum of the diffraction peak and θ is the diffraction angle. The D values obtained from XRD are depicted in Fig. 2. It is clear that the grain size D values decreased with increasing the Co^{2+} concentration, indicating that cobalt doping have a regulating effect on grain size.

Figures 3 and 4a show the TEM micrograph of the $Zn_{1-x}Co_xAl_2O_4$ (x = 0 and 0.20) samples. From the typical images, it can be seen that the $ZnAl_2O_4$ sample consists of dispersed nanoparticles. It is not difficult to find that, compared with the samples without doping, the Co doped samples can be obtained with smaller particle size and uniform size distribution. It is thus clear that cobalt doping affects the morphology of the sample. According to Figs. 3 and 4, the average size is about 18.3 and 12 nm, respectively for pure $ZnAl_2O_4$ and $Zn_{0.8}Co_{0.2}Al_2O_4$. The results were consistent with the XRD results.

Figures 3 and 4b show HREM images of the samples. The interplanar spacing values of $Zn_{1-x}Co_xAl_2O_4$ (x = 0 and 0.20) are 0.2838 and 0.2825 nm, respectively. It is in a good agreement with the d-spacing of (220) planes of the cubic $ZnAl_2O_4$. The lattice spacing value of $Zn_{0.8}Co_{0.2}Al_2O_4$ is smaller than that of pure $ZnAl_2O_4$, which due to the radius of Co^{2+} (0.072 nm) smaller than radius of Zn^{2+} (0.074 nm). So after being doped with Co^{2+}, the lattice distortion occurred.

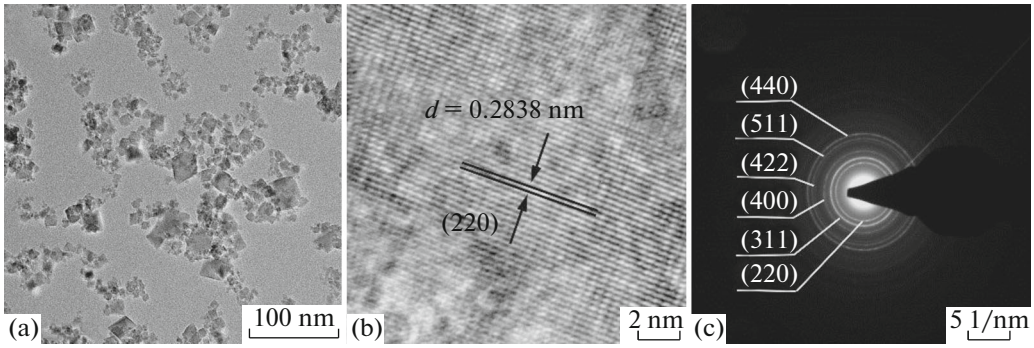

Fig. 3. TEM images and selected area diffraction pattern of $ZnAl_2O_4$ sample.

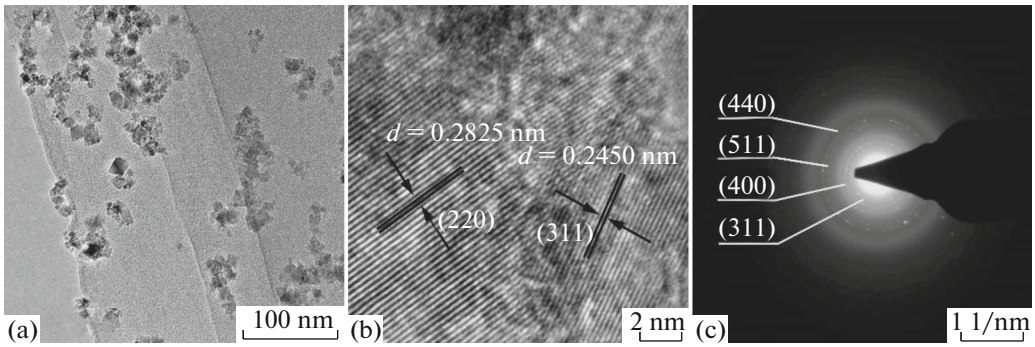

Fig. 4. TEM images and selected area diffraction pattern of $Zn_{0.8}Co_{0.2}Al_2O_4$ sample.

The selected area electron diffraction (SAED) patterns are shown in the Figs. 3c and 4c. The polycrystalline diffraction rings being indexed to the crystal planes (220), (311), (400), (331), (422), (511), (440), (620), and (533) of $ZnAl_2O_4$, respectively, which showed that the samples exhibited zinc aluminate spinel structure. There were no additional diffraction rings and spots of second phases. The SAED patterns confirm that the $Zn_{1-x}Co_xAl_2O_4$ ($x = 0$ and 0.20) nanoparticles are of cubic spinel structure.

Figures 5a, 5b show EDX spectra of $Zn_{1-x}Co_xAl_2O_4$ ($x = 0$ and 0.2). The peaks corresponding to Zn, Al, and O were observed in pure $ZnAl_2O_4$ (Fig. 5a); C and Cu come from the copper grid. In Fig. 5b, besides Zn, Al, O, C, and Cu, cobalt was also observed in the Co-doped $ZnAl_2O_4$ sample. Therefore, the EDX spectrum shows that Co was detected in 20% sample.

Figure 6 shows FT-IR spectra of all samples recorded in 400–4000 cm^{-1} range. The band at 3456 cm^{-1} can be assigned to vibration mode of chemically bonded hydroxyl groups. The band at 1635 cm^{-1} corresponds to the deformation vibration of water molecule. The weak vibration modes at the band of 1350 to 1550 cm^{-1} can be assigned to the organic compounds (CTAB or alcohol) induced at the preparation of the sample [15]. The bands at 680, 550, and 493 cm^{-1} are dependent on the Al–O stretching mode, Zn–O stretching mode and Al–O bending mode, respectively. These bands are the characteristic of regular zinc aluminate spinel structure, in accordance with literature data [12, 16, 17]. The result is agreement with XRD results for the samples of $Zn_{1-x}Co_xAl_2O_4$ ($x = 0$, 0.10, 0.20, and 0.40). Finally, with the increasing of doped Co^{2+} ions in the samples, these mode peaks show a more broaden and weakened trend. It is generally ascribed to the decreased grain size D.

To obtain information on the chemical binding states of ions in our samples, X-ray photoelectron spectroscopy (XPS) has been performed (Figs. 7–10). All binding energies have been corrected using the adventitious C1s photoelectron signal at 284.8eV.

In Fig. 7, the Zn 2p core level spectrum is characterized by two components appearing due to the spin-orbit splitting between Zn $2p_{3/2}$ and Zn $2p_{1/2}$, whose binding energies are 1022 and 1045.2 eV, respectively. The binding energy differences between the two lines are 23.2 eV, which is lying close to the standard reference value of $ZnAl_2O_4$ [15, 18]. In Fig. 8, the Al 2p peak of the sample were observed at about 74.0 eV. The

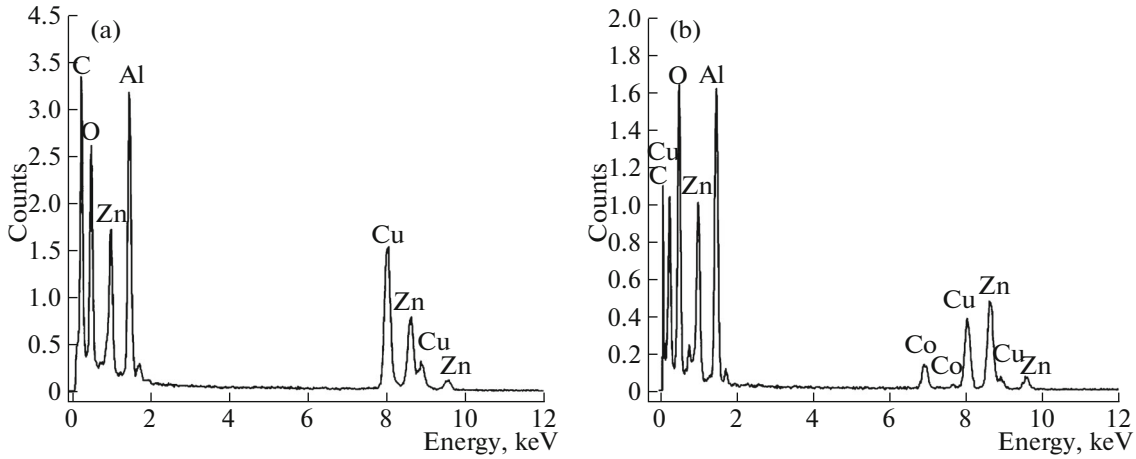

Fig. 5. EDX spectra of $ZnAl_2O_4$ (a) and $Zn_{0.8}Co_{0.2}Al_2O_4$ (b) samples.

binding energy of the Al 2*p* signal is compatible with the presence of Al^{3+} species. The result is identical with the reported in literature [19].

The O 1*s* XPS signals shown in Fig. 9 are divided into three peaks at about 531.1, 532.5, and 533.7 eV for $Zn_{1-x}Co_xAl_2O_4$ (x = 0. 0.20, and 0.40) samples. The main peaks centered at 531.1 eV are attributed to the contribution of the crystal lattice oxygen. The peaks centered at 532.5 eV most likely relate to oxygen deficiency, indicating there are some oxygen vacancies in the samples; the peaks centered at 533.7 eV are usually attributed to the presence of loosely bound oxygen on the surface or hydrated oxide species such as adsorbed contaminants, chemisorbed oxygen species, $-CO_3$, H_2O, and O_2 [20, 21]. The oxidation states of Co were investigated by measuring the Co 2*p* XPS spectra, as shown in Fig. 10. The Co $2p_{3/2}$ XPS spectra are well fitted into three peaks situated on 779.8, 781.1, and 786.1 eV for 20%, 780.0, 781.2, and 786.7 eV for 40%, respectively. The signals at 786.1 and 786.7 eV are characterized to be the satellite peak of Co $2p_{3/2}$ main line.

The peaks at lower (779.8 and 778.0 eV) and higher binding energies (781.1 and 781.2 eV) are assigned to Co ions in octahedral sites and tetrahedral sites for two samples, respectively. The Co 2*p* XPS results clearly show that the Co ions mainly occupied the tetrahedral site and its local site occupancy changes to the octahedral site.

Figure 11 shows the room temperature PL spectra of Co doped $ZnAl_2O_4$ samples recorded at the excitation wavelength of 254 nm. In Fig. 11, a blue emission peak centered at 458, 458.3, 459, and 459.5 nm for $Zn_{1-x}Co_xAl_2O_4$ (x = 0, 0.10, 0.20, and 0.40) samples respectively is associated with oxygen vacancies (V_O) [22–24]. With Co^{2+} concentration increasing,

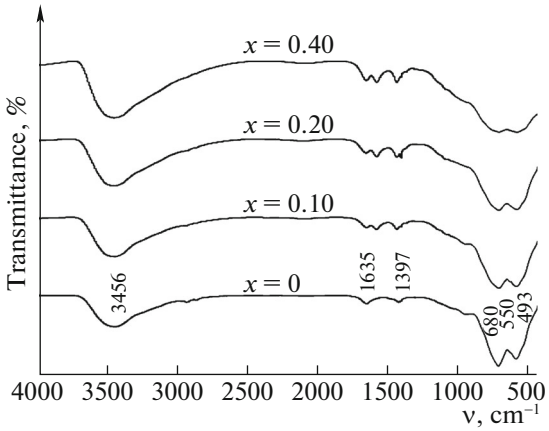

Fig. 6. FT-IR spectra of $Zn_{1-x}Co_xAl_2O_4$ (x = 0, 0.10, 0.20, and 0.40) samples.

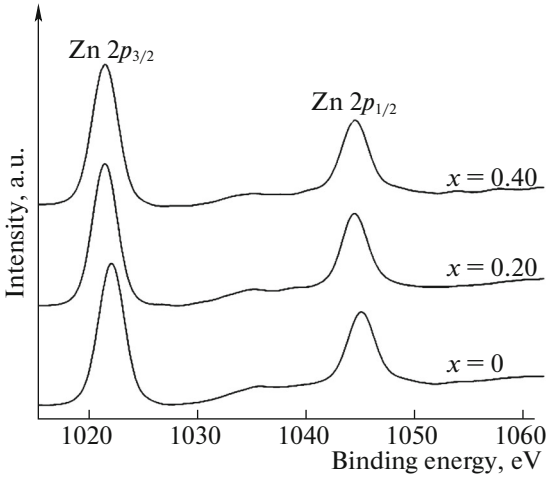

Fig. 7. XPS spectra of Zn2*p* of $Zn_{1-x}Co_xAl_2O_4$ (x = 0, 0.20, and 0.40) samples.

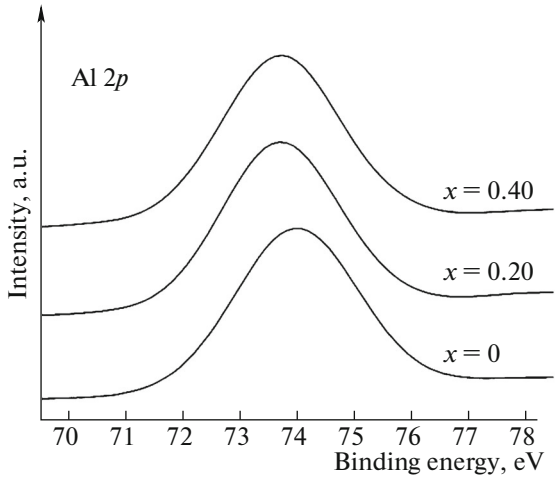

Fig. 8. XPS spectra of Al 2*p* of $Zn_{1-x}Co_xAl_2O_4$ (x = 0, 0.20, and 0.40) samples.

the blue emission peaks of Co-doped samples are red-shifted, compared to pure $ZnAl_2O_4$. The red shift can be explained by the following reasons. From the XRD results, the grain size of samples decreased as the Co^{2+} content increased, the particle internal stress increases. The factor makes energy level spacing decreases causing the red-shift.

Figure 12 shows the UV–Vis absorbance spectra of all samples recorded in the range of 230–850 nm. The absorption band in the wavelength range of 500–750 nm, a three-structured band at about 545, 592, and 638 nm, which is the characteristic of Co^{2+} ions in the tetrahedral sites, is observed [12].

This absorption could be easily assigned to the $^4A_2(F) \rightarrow {}^4T_1(P)$ spin allowed transition for the Co^{2+} located in tetrahedral sites. No features characteristic of octahedral Co^{2+} ions were registered in absorption spectra. Its structured pattern is resulted

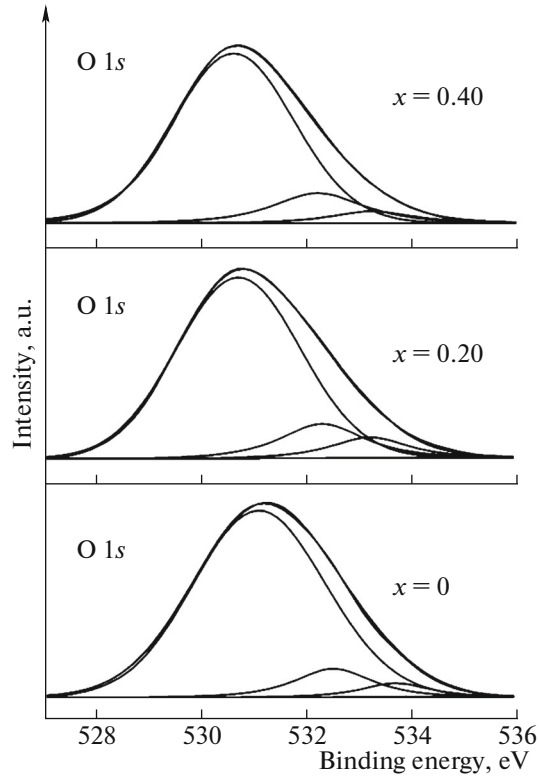

Fig. 9. XPS spectra of O 1*s* of $Zn_{1-x}Co_xAl_2O_4$ (x = 0, 0.20, and 0.40) samples.

most probably from the significant effects of the spin-orbit coupling which split the ^4T state in three spinor components, usually occurring as a triplet around 545 nm (green region), 592 nm (yellow-orange region), 638 nm (red region) that results in the blue coloration of the samples [25].

Due to both the Co^{2+} (0.072 nm) and Zn^{2+} (0.074 nm) have similar the ionic radii and the valence state, the

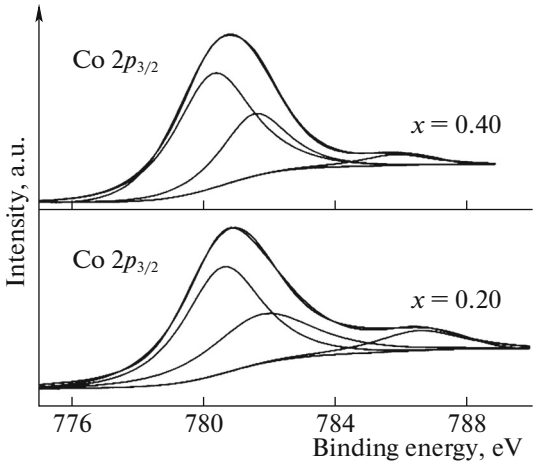

Fig. 10. XPS spectra of Co 2*p* of $Zn_{1-x}Co_xAl_2O_4$ (x = 0.20 and 0.40) samples.

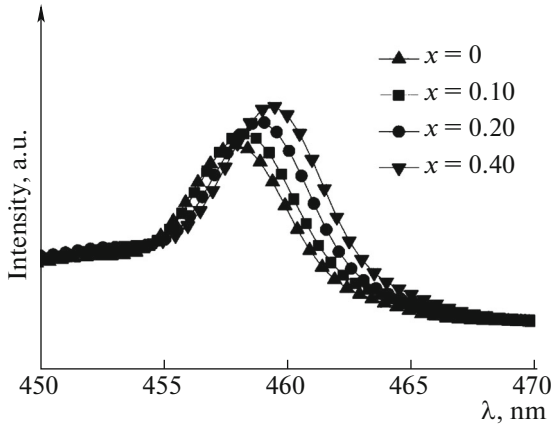

Fig. 11. PL spectra of $Zn_{1-x}Co_xAl_2O_4$ (x = 0, 0.10, 0.20, and 0.40) samples.

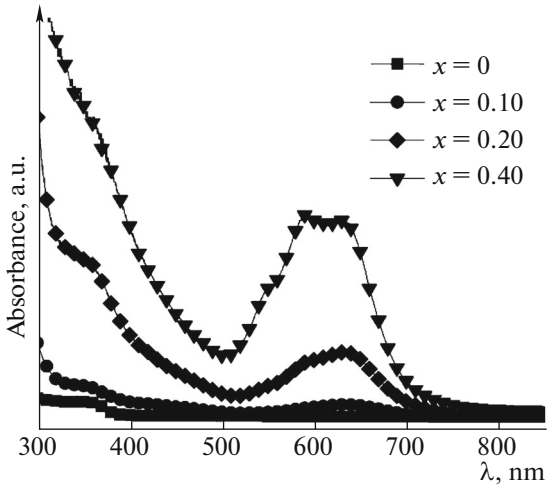

Fig. 12. UV–Vis spectra of $Zn_{1-x}Co_xAl_2O_4$ (x = 0, 0.10, 0.20, and 0.40) samples.

Co^{2+} ions more easily substitute Zn^{2+} ions rather than the Al^{3+} in the $ZnAl_2O_4$ crystalline structure from 0 to 40%. With the increase of Co ions concentration, the peaks intensity of this three bands gradually enhanced. The UV–Vis spectra results indicate that more and more Co^{2+} ions substituted for Zn^{2+} ions without changing the spinel structure.

CONCLUSIONS

Co-doped $ZnAl_2O_4$ nanoparticles were successfully prepared by hydrothermal method. The samples possess cubic spinel structure, no other impurity phases were observed. Cobalt doping has a regulating effect on grain size, the average grain size of the Co doped samples decreases with the increase of Co^{2+} concentration. Due to the grain size decreased, the FT-IR broadened in the low frequency band and the PL results showed that the peaks have the red-shift. The UV–Vis spectra results showed that more and more Co^{2+} ions substituted for Zn^{2+} ions without changing the spinel structure.

ACKNOWLEDGMENTS

This work was supported by the National Natural Science Foundation of China (no. 51261015) and the Natural Science Foundation of Gansu Province, China (no. 1308RJZA238).

REFERENCES

1. M. Chabo, E. Pellicer, E. Rossinyol, O. Castell, S. Surinach, and M. D. Baro, Cryst. Growth Des. **9**, 4814 (2009).
2. Q. Song and Z. John Zhang, J. Am. Chem. Soc. **126**, 6164 (2004).
3. F. Tielens, M. Calatayud, R. Franco, J. M. Recio, J. Pérez-Ramirez, and C. Minot, J. Phys. Chem. B **110**, 988 (2006).
4. K. Izumi, S. Miyazaki, S. Yoshida, T. Mizokawa, and E. Hanamura, Phys. Rev. B **76**, 075111 (2007).
5. A. Goldstein, Y. Yeshurun, M. Vulfson, and H. Kravits, J. Am. Ceram. Soc. **95**, 879 (2012).
6. F. Y. Zhang, Z. Zeng, and J. Q. You, J. Nanosci. Nanotechnol. **10**, 5475 (2010).
7. R. T. Kumara, N. C. S. Selvama, C. Ragupathia, L. J. Kennedyb, and J. J. Vijaya, Powder Technol. **224**, 147 (2012).
8. L. Cornu, M. Gaudon, and V. Jubera, J. Mater. Chem. C **1**, 5419 (2013).
9. W. Lei, W. Z. Lu, D. Liu, and J. H. Zhu, J. Am. Ceram. Soc. **92**, 105 (2009)
10. X. L. Duan, D. R. Yuan, Z. H. Sun, C. N. Luan, D. Y. Pan, D. Xu, and M. K. Lv, J. Alloys Compd. **386**, 311 (2005).
11. D. Zhang, C. Z. Wang, Y. L. Liu, Q. Shi, W. J. Wang, and Y. Zhai, J. Lumin. **132**, 1529 (2012).
12. G. T. Anand, L. J. Kennedy, and J. J. Vijaya, J. Alloys Compd. **581**, 558 (2013).
13. D. Zhang, Y. L. Yin, Y. L. Liu, W. B. Chao, and Y. Zhai, J. Phys. Chem. Solids **74**, 1131 (2013).
14. X. J. Wang, M. Zhang, H. Ding, and Z. Sun, J. Alloys Compd. **509**, 6317 (2011).
15. Z. R. Zhu, X. Y. Lia, Q. D. Zhao, S. M. Liu, X. J. Hu, and G. H. Chen, Mater. Lett. **65**, 194 (2011).
16. R. Ianoş, Radu Lazău, Ioan Lazău, and C. Păcurariu, J. Eur. Ceram. Soc. **32**, 1605 (2012).
17. S. D. Kapse, F. C. Raghuwanshi, V. D. Kapse, and D. R. Patil, Curr. Appl. Phys. **12**, 307 (2012).
18. L. Zhang, J. H. Yan, M. J. Zhou, Y. H. Yang, and Y. N. Liu, Appl. Surf. Sci. **268**, 237 (2013).
19. S. Iaiche and A. Djelloul, J. Spectrosc. **2015**, 1 (2015).
20. W. P. Wang, H. Yang, T. Xian, and J. L. Jiang, Mater. Trans. **53**, 1586 (2012).
21. V. Kumar, H. C. Swart, O. M. Ntwaeaborwa, R. E. Kroon, J. J. Terblans, S. K. K. Shaat, A. Yousif, and M. M. Duvenhage, Mater. Lett. **101**, 57 (2013).
22. X. Q. Wei, B. Y. Man, M. Liu, C. S. Xue, H. Z. Zhuang, and C. Yang, Physica B **388**, 145 (2007).
23. H. X. Chen, J. J. Ding, X. G. Zhao, and S. Y. Ma, Physica B **405**, 1339 (2010).
24. D. H. Zhang, Z. Y. Xue, and Q. P. Wang, J. Phys. D: Appl. Phys. **35**, 2837 (2002).
25. D. Visinescu, C. Paraschiv, A. Ianculescu, B. Jurca, B. Vasile, and O. Carp, Dyes Pigm. **87**, 125 (2010).